Journal of Hazardous Materials 211–212 (2012) 389–395

Contents lists available at ScienceDirect

Journal of Hazardous Materials

journal homepage: www.elsevier.com/locate/jhazmat

Vertically aligned Ag nanoplate-assembled film as a sensitive and reproducible SERS substrate for the detection of PCB-77

Chuhong Zhu [a], Guowen Meng [a,*], Qing Huang [b,*], Zhulin Huang [a]

[a] Key Laboratory of Materials Physics, and Anhui Key Laboratory of Nanomaterials and Nanostructures, Institute of Solid State Physics, Chinese Academy of Sciences, Hefei 230031, China
[b] Key Laboratory of Ion Beam Bioengineering, Hefei Institutes of Physical Science, Chinese Academy of Sciences, Hefei 230031, China

ARTICLE INFO

Article history:
Received 25 March 2011
Received in revised form 21 June 2011
Accepted 27 July 2011
Available online 10 August 2011

Keywords:
SERS
Detection
PCBs
Ag nanoplate
Sensitive
Reproducible

ABSTRACT

Vertically aligned Ag nanoplate-assembled film has been achieved by spin-coating Ag seeds on an ITO substrate and subsequent electrodeposition in a mixed aqueous solution of $AgNO_3$ and citric acid. As sufficient hot spots are located in the deep gaps between the neighboring nanoplates across the whole substrate, the Ag nanoplate-assembled film shows strong Surface enhanced Raman scattering (SERS) effect, together with good signal reproducibility. Therefore, the Ag nanoplate-assembled films were tried as robust, highly sensitive and reproducible SERS substrates for the rapid detection of 3,3′,4,4′-tetrachlorobiphenyl (PCB-77) and a detection limit of about 10^{-6} M was reached. For further reducing the detection limit, a layer of decanethiol was modified on the Ag nanoplate surface to capture the PCB-77 molecules efficiently, and a lower detection limit of 10^{-7} M was achieved. A linear dependence was found between the logarithmic concentrations of PCB-77 and the intensities of the fingerprint peaks. Furthermore, the Ag nanoplate-assembled film can also be used as a SERS substrate to distinguish characteristic peaks of different polychlorinated biphenyls (PCBs) in their mixed solutions. Therefore the vertically aligned Ag nanoplate-assembled film has potentials as effective SERS substrates in rapid and direct detection of trace PCBs.

1. Introduction

Polychlorinated biphenyls (PCBs) were heavily used from the 1930s to the 1970s in industry, mainly as insulation in electrical transformers [1]. As no effective control on waste disposal during that period, PCBs spread throughout the environment. Awareness of PCBs' presence in the environment and their toxicity to human and wildlife lead to a ban in 1979 on sale and production [2]. But PCBs can still be found today in high concentrations in snow [3], soils [4], waste disposal sites, natural waters, and in the aquatic life of these waters [5–10]. PCBs can cause harmful biological effects, such as toxicity, mutagenicity, carcinogenicity, and endocrine disrupter activity [5,11–14]. PCBs can bio-accumulate in fatty tissues through food chains [10], so even small exposures may eventually reach dangerous levels. Rapid and sensitive detection of PCBs is therefore extremely important. Traditional techniques for detecting PCBs mainly include high-resolution capillary gas chromatographic columns with an electron capture detector [15,16], immunoassays [17], ion detection technique [18], and high-resolution mass spectrometry [16]. But these methods are generally costly and time-consuming.

Surface-enhanced Raman scattering (SERS) has attracted great interest due to its high sensitivity in trace molecular detection [19]. The noble metal (especially Au and Ag) nanometer-scale gaps [20], sharp tips [21] and edges [22] are believed to have highly concentrated electromagnetic fields associated with strong localized surface plasmon resonance (LSPR) so that "hot spots" occur at these positions. For an effective SERS substrate, it is generally required to have not only enough hot spots to ensure high sensitivity, but also uniformity of the substrate to ensure good reproducibility for SERS measurements in practice. To achieve high sensitivity and reproducibility of SERS substrates, nanoparticle colloids [23,24] and periodic nanostructures [25,26] have been developed. Nanoparticle colloids can induce enormously enhanced SERS signal at some local hot spots due to the aggregation of the colloids, but it is difficult to achieve reproducibility because it is hard to ensure the hot spots to be homogenously distributed on the substrate. Nanometer-scale lithography techniques can be used to fabricate periodic nanostructures with a moderate enhancement (10^5–10^6) and high reproducibility [23], but they are usually expensive. Moreover, both theoretical and experimental studies prove that the control of gaps between nanostructures on SERS substrates in the sub-10-nm regime is very critical to

* Corresponding author.
E-mail addresses: gwmeng@issp.ac.cn (G. Meng), huangq@ipp.ac.cn (Q. Huang).

0304-3894/$ – see front matter © 2011 Elsevier B.V. All rights reserved.
doi:10.1016/j.jhazmat.2011.07.118

attain optimum SERS effect [20,26–28]; however the fabrication of uniform and dense periodic gaps in such a small scale remains a big challenge.

Previously, we achieved arrays of Ag nanosheet-assembled micro-hemispheres that were successfully used as highly sensitive and reproducible SERS substrates for the detection of 3,3′,4,4′-tetrachlorobiphenyl (PCB-77) [29]. In that case we had to "see" one of the hemispheres first under the optical microscopy of the confocal microprobe Raman system, and then measured Raman signals from the observed micro-hemisphere. If the density of the Ag micro-hemispheres is high enough to form a compact film of Ag micro-hemispheres or vertically aligned nanoplates, the structural uniformity of the whole substrate could be much improved, and it would be much easier for SERS measurement in practical applications. Based on these ideas, here we present a low-cost and simple Ag seed-assisted electrodeposition on indium tin oxide (ITO) substrates for the fabrication of large-area compact films consisting of vertically aligned Ag nanoplates with sufficient deep sub-10-nm gaps between the neighboring nanoplates. As sufficient hot spots are located in the deep gaps between the neighboring nanoplates across the whole substrate, the Ag nanoplate-assembled film shows strong SERS effect, together with good reproducibility. Therefore, the as-prepared Ag nanoplate-assembled films can serve as cost-effective, sensitive, reproducible and robust SERS substrates for rapid trace detection of persistent organic pollutants such as PCB-77. As PCBs cannot be easily adsorbed onto the surface of Ag nanoplate-assembled film, in this work, a partition layer (decanethiol self-assembled layer) was assembled onto the SERS substrate to concentrate the target PCB molecules within the surfaces of the SERS substrate through its efficient van der Waals interactions with the hydrophobic PCBs. It is demonstrated that the detection limit of PCB-77 can be really reduced by decanethiol modification on the surface of the Ag nanoplate-assembled film.

Compared with the previously reported SERS substrate consisting of Ag nanosheet-assembled micro-hemispheres [29], now we can randomly choose a spot on the film to get SERS signals rather than have to "see" one micro-hemisphere before getting SERS signals, since this new SERS substrate is made up of a large area film consisting of uniformly and densely distributed Ag nanoplates on an ITO substrate. In addition, the lower detection limit of PCB-77 achieved by using the Ag nanoplate-assembled film modified with decanethiol as a SERS substrate (10^{-7} M) is even lower than that obtained by using Ag nanosheet-assembled micro-hemispheres (3×10^{-6} M). Although aligned Ag nanorods were also used as a SERS substrate for the detection of 2,3,3′,4,4′-pentachlorinated biphenyl, however there appeared some unexplained bands in the SERS spectra [30].

2. Experimental

2.1. Apparatus and reagents

The resultant compact Ag nanoplate-assembled film was characterized by using X-ray diffraction (XRD) (Philips X'pert-PRO), scanning electron microscope (SEM, Hitachi S-4800), transmission electron microscope (TEM, JEOL 2010) and Ultraviolet–Visible-Near-Infrared spectrophotometer (Hitachi, U-4100). The compact Ag nanoplate-assembled films were cleaned by using a plasma cleaner (PDC-32G, high power) for 10 min, and then used as SERS substrates. SERS measurement was conducted on a confocal microprobe Raman system (Renishaw, inVia) with the excitation wavelength of 532 nm. During SERS measurement, the laser light was vertically projected onto the samples with a resultant beam diameter of ~5 μm.

The reagents, sodium citrate, citric acid, R6G, PCB-77, $NaBH_4$, and $AgNO_3$ were analytical grade.

2.2. Preparation of the Ag nanoplate-assembled film

The film comprising vertically aligned Ag nanoplates on an ITO substrate was fabricated via spin-coating Ag seeds on the ITO substrate and subsequent electrodeposition in a mixed aqueous solution of $AgNO_3$ and citric acid, as shown schematically in Fig. 1. Silver colloidal solution was first prepared. Typically, 0.5 mL of 60 mM $AgNO_3$ and 1 mL of 35 mM sodium citrate were added to 98 mL of deionized (DI) water. The mixed solution was stirred for several minutes. Then, 0.5 mL of an aqueous 20 mM $NaBH_4$ solution, which had been aged at room temperature for 2 h, was added quickly, stirred for 1 h and then aged at room temperature for 24 h before use. ITO substrates (1 cm × 2 cm) were ultrasonically cleaned in acetone and then in ethanol for 1 h, respectively. A droplet of the prepared Ag colloidal solution (0.1 mL) was spin-coated on the cleaned substrate on a custom-built spin coater. The coating area on the substrate was fixed to be about 1 cm in diameter. After that, the substrate was dried at 40 °C. For the synthesis of Ag nanoplate-assembled film, 0.1 g $AgNO_3$ and 0.9 g citric acid were added to 50 mL DI water, followed by stirring until complete dissolution of the solute. Such an aqueous solution was used as the electrolyte in the electrodeposition. A rectangular graphite sheet was used as anode and a piece of ITO glass (2 cm × 0.5 cm) spin-coated with Ag seeds was used as cathode, respectively. The electrodeposition of the Ag nanoplate-assembled film was carried out under a constant current density of 170 μA cm^{-2} for 20 min at room temperature. The ITO glass with the electrodeposited products was then taken out, cleaned with DI water several times and dried with high-purity flowing nitrogen.

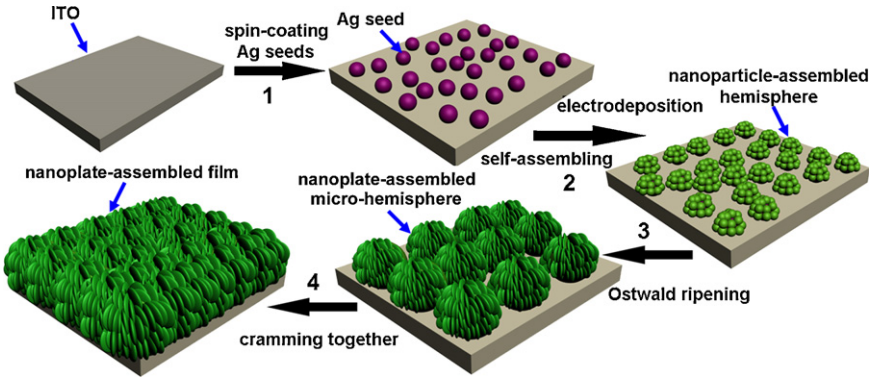

Fig. 1. Schematic for the fabrication of vertically aligned Ag nanoplate-assembled film. (1) Spin-coating Ag-seeds on an ITO substrate. (2) Ag seed-assisted electrodeposition of Ag nanoparticle-assembled hemispheres. (3) Transformation of Ag nanoparticle-assembled hemispheres into nanoplate-assembled micro-hemispheres by Ostwald ripening. (4) Ag nanoplate-assembled micro-hemispheres cramming together to form vertically aligned Ag nanoplate-assembled film.

2.3. General procedure

To ensure good molecule adsorption, the Ag nanoplate-assembled films on ITO substrates (0.3 cm × 0.3 cm) were immersed in 1.5 mL rhodamine 6G (R6G) solutions (10^{-6} and 10^{-15} M aqueous solution) for 2 h, taken out and then dried with high-purity flowing nitrogen. For the estimation of enhancement factor for R6G, 10 μL of a 3×10^{-3} M R6G ethanol solution was dispersed on a glass, and formed a spreading area of 10 mm in diameter, and 10 μL of a 10^{-11} M R6G solution was dispersed to 15 mm^2 Ag nanoplate-assembled film and dried in high-purity argon. For PCB-77 detection, the PCB-77 solution (4 μL) was dripped 10 times (with about 0.4 μL each time) on the substrate. The droplets formed circular patterns with an average diameter of about 0.2 cm in the middle of the substrates. For further effective capture of PCB-77, the Ag nanoplate-assembled films were placed in 1 mL of a 1 mM ethanolic 1-decanethiol solution for 10 min. Afterwards the Ag nanoplate-assembled films were removed, rinsed with ethanol, and allowed to dry in the blow of high-purity Ar. Then 4 μL aliquots from 10^{-4}, 10^{-5}, 3×10^{-6}, 10^{-6} and 10^{-7} M solutions were dispersed to five pieces of decanethiol-modified Ag nanoplate-assembled film substrates (0.3 cm × 0.3 cm) and dried in a fuming cupboard.

3. Results and discussion

3.1. Characterization of the Ag nanoplate-assembled film

Typical SEM images of the as-prepared Ag nanoplate-assembled film with different magnifications are presented in Fig. 2a–e. These SEM images indicate that the Ag film (with a thickness of about 300 nm) is composed of a large number of nanoplates with an average thickness of about 20 nm and with sufficient deep sub-10-nm gaps between neighboring nanoplates. X-ray diffraction spectrum (Fig. 1h) taken from the Ag film displays four peaks of Ag crystal, which correspond to the diffractions from the (1 1 1), (2 0 0), (2 2 0) and (3 1 1) planes of the face-centered-cubic (fcc) phase respectively, confirming that the resultant nanoplates are well crystallized Ag crystals. Transmission electron microscopy observation (Fig. 1f and g) on a nanoplate further indicates that the Ag nanoplate is well crystallized. The corresponding selected area electron diffraction (SAED) pattern (inset in Fig. 1f) reveals that the planar surface of the nanoplate is parallel to {1 1 1} planes of the fcc phase Ag, since electron beam was perpendicular to the surface of the nanoplate. The UV–vis spectrum of the Ag nanoplate-assembled film reveals the plasmon absorption band peak at 381 nm (Fig. 1i).

3.2. Formation of the Ag nanoplate-assembled film

In order to reveal the formation process of the Ag nanoplate-assembled film in detail, experiments were conducted for various electrodeposition durations of 1 s, 30 s, 2 min, 5 min, 10 min, and 25 min. Representative SEM observations on the obtained products with different electrodeposition durations are shown in Fig. 3. Nanoparticle-assembled micro-hemispheres were formed after electrodeposition for 1 s or 30 s (Fig. 3a and b). When the electrodeposition duration was prolonged to 2 min, the nanoparticles were beginning to transform into nanoplates (Fig. 3c). After the electrodeposition was prolonged to 5 min, the micro-hemispheres were composed of nanoplates (Fig. 3d). After the electrodeposition was further prolonged to 10 min, the micro-hemispheres began

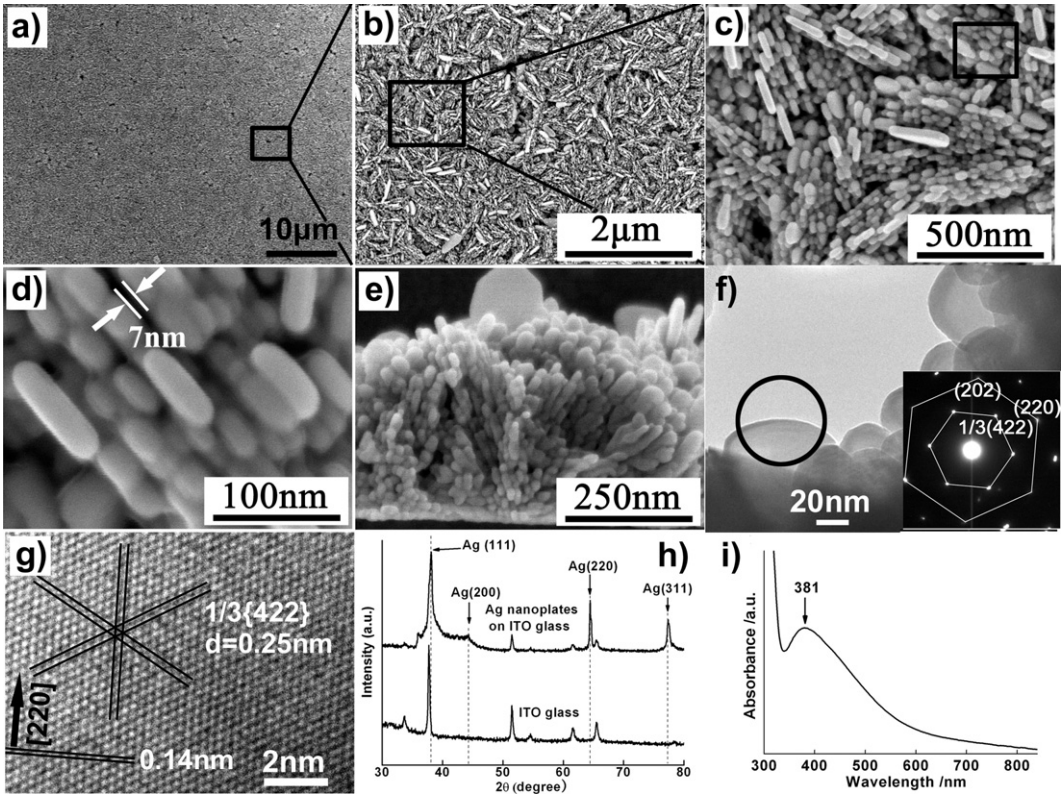

Fig. 2. (a)–(c) SEM images of the Ag nanoplate-assembled film (achieved via electrodeposition for 20 min) at different magnifications. (d) Close-up view of the rectangular region marked in (c). (e) SEM side view of the nanoplate-assembled film. (f) TEM image of the Ag nanoplates, the inset is the SAED pattern from the circled area. (g) High-resolution TEM image of the nanoplate in the circled area in (f). (h) XRD spectra taken from the ITO glass with (top) and without (bottom) the Ag nanoplate-assembled film. (i) The UV–vis spectrum of the Ag nanoplate-assembled film.

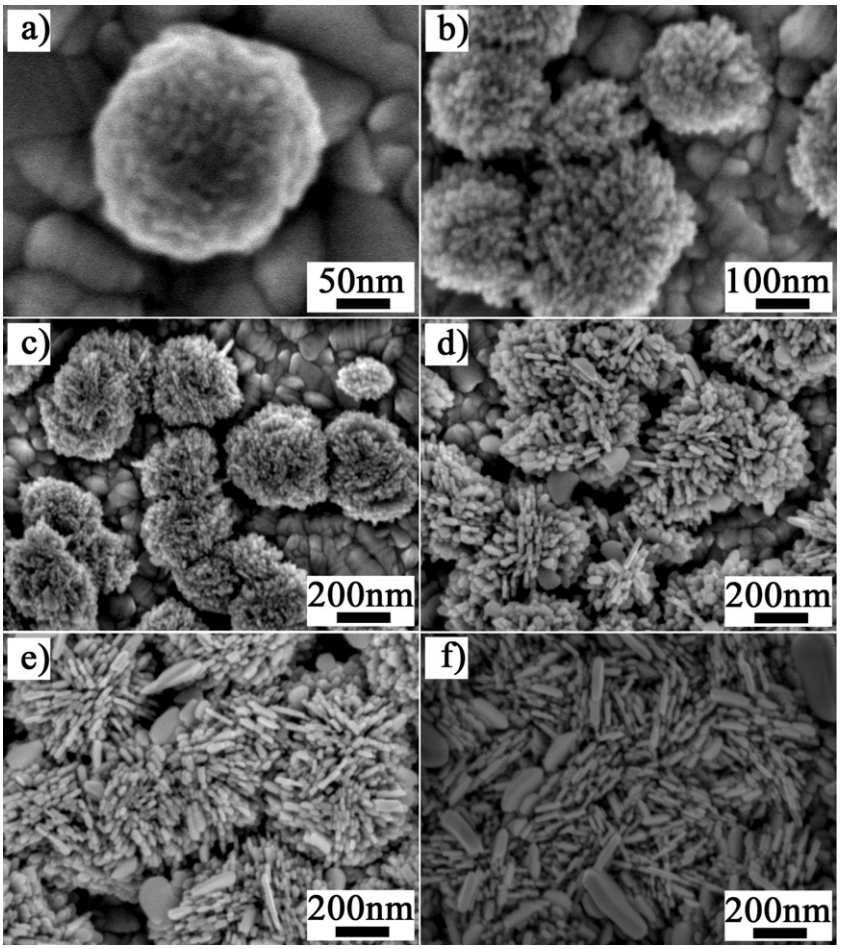

Fig. 3. SEM images of products electrodeposited for (a) 1 s, (b) 30 s, (c) 2 min, (d) 5 min, (e) 10 min and (f) 25 min, respectively.

to crowd together (Fig. 3e). When the electrodeposition duration was prolonged to 20 min, the ITO substrate would be cram-full of vertically aligned nanoplates and there appeared a film composed of vertically aligned nanoplates (Fig. 2b). If the electrodeposition duration was prolonged much longer to 25 min, the film would be composed of larger nanoplates (Fig. 3f). Based on the above detailed SEM observations, the formation of the nanoplate-assembled film can be explained as follows. In a typical experiment, under the electric field, Ag^+ ions in the electrolyte move to the surface of the cathode (ITO substrate) and the following reduction reaction takes place:

$$Ag^+ + e \rightarrow Ag^0 \quad (1)$$

The reduced Ag^0 atoms form Ag clusters or particles and then attach themselves onto the Ag seeds that were spin-coated on the ITO glass beforehand. In the meantime, citric acid that acts as a stabilizer can bind to the particle surfaces [31–35]. The absorbed citric acid retards the growth of the particles, and the up-coming continually reduced Ag^0 atoms lead to the formation of new particles. These particles then form nanoparticle-assembled hemispheres by self-assembling (step 2 in Fig. 1). We suggest that an oriented attachment progress dominates the self-assembling of the micro-hemispheres, where different particles are involved in attachment, rotation, and realignment [36,37]. In the oriented attachment progress, nanoparticles fuse together with high-energy surfaces under crystallographic fusion, which eliminates high-energy faces [38]. Then, at the following stage (after 2 min), Ostwald ripening plays an important role in the formation of smooth and regular nanoplates [39], so that micro-hemispheres composed of layered nanoplates are formed (step 3 in Fig. 1). At the final stage, the continuing growth of the micro-hemispheres will lead to their cramming together to form Ag nanoplate-assembled film (step 4 in Fig. 1).

3.3. SERS performance

The SERS performance of the nanoplate-assembled film was tested by using R6G that is one of the most common organics used for checking the performance of SERS substrates. The SERS spectra of R6G at different concentrations on the films are shown in Fig. 4a. Many bands are distinctly observed in the spectra even when the R6G concentration was reduced down to 10^{-15} M, showing high sensitivity of the Ag nanoplate-assembled film for SERS detection. The most pronounced bands appear at 612 (C–C–C ring in-plane vibration), 775 (C-C-C ring out-of-plane bending), and 1362 (aromatic C–C stretching) cm^{-1} [40,41].

The average SERS enhancement factor (EF) of the Ag nanoplate-assembled film was calculated by comparing the peak intensities of SERS signals from R6G molecules on the Ag nanoplate-assembled film (curve II in Fig. 4a) to those of the corresponding signals from the R6G film on a reference glass substrate (curve I in Fig. 4a) according to the following formula [42,43]:

$$EF = \frac{I_{SERS} N_{Ref}}{I_{Ref} N_{SERS}} \quad (2)$$

where I_{SERS} and I_{Ref} are Raman intensities, N_{SERS} and N_{Ref} are the number of molecules for "SERS" and "Ref" (stands for "reference") samples, respectively. For the pure R6G film with an area of 10 mm^2,

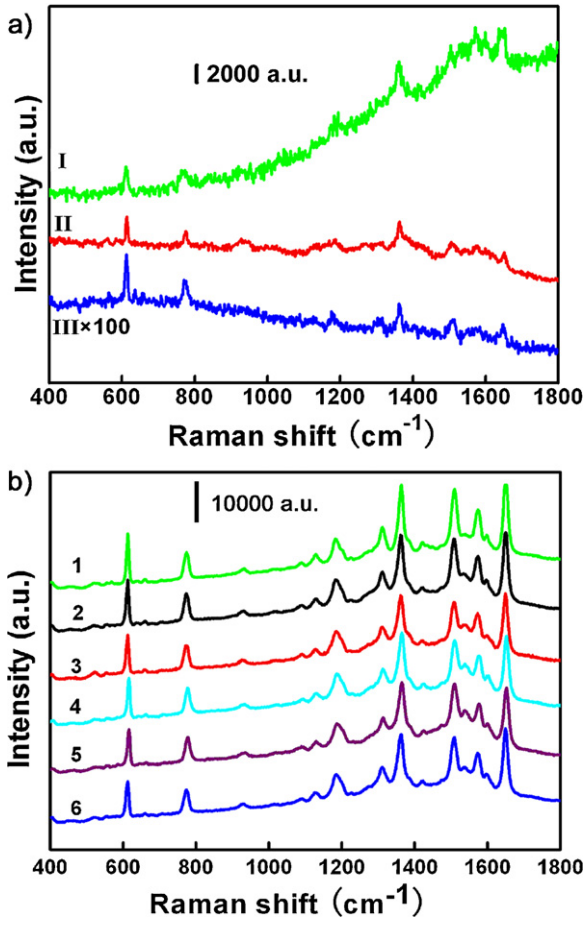

Fig. 4. (a) Curve I: normal Raman spectrum for a R6G film, Curves II and III: SERS spectra of R6G on Ag nanoplate-assembled film with the R6G concentrations of 10^{-11} and 10^{-15} M, respectively. All the spectra were acquired with the acquisition time of 3 s. (b) SERS spectra of 10^{-6} M R6G from six randomly chosen spots on the Ag nanoplate-assembled film with acquisition time of 2 s.

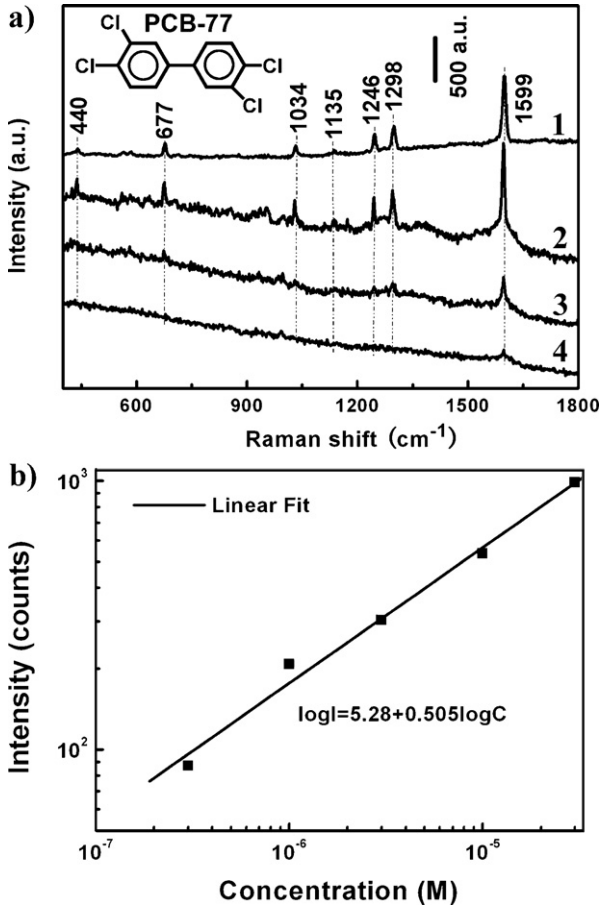

Fig. 5. (a) Curve 1: normal Raman spectrum for pure PCB-77 powder and curves 2–4: SERS spectra of 10^{-4}, 3×10^{-6} and 3×10^{-7} M PCB-77 from Ag nanoplate-assembled film, respectively. All the spectra were acquired with acquisition time of 60 s. (b) The linear relationship between the logarithmic intensities (1599 cm^{-1}) and the concentrations of PCB-77 detected by using the bare Ag nanoplate-assembled film.

considering the laser spot is a circle with a diameter of 5 μm, the number of the R6G molecules illuminated by the laser (N_{Ref}) is $3 \times 10^{-3} \times 10^{-5} \times 6.02 \times 10^{23} \times \pi(5\,\mu m/2)^2/10\,mm^2 = 3.5 \times 10^{10}$. For the estimation of N_{SERS} and I_{SERS}, 10 μL of a 10^{-11} M R6G aqueous solution was dispersed to 15 mm^2 of the Ag nanoplate-assembled film. Supposing that all R6G molecules are absorbed on the Ag nanoplate-assembled film, N_{SERS} was estimated to be $10^{-11} \times 10^{-5} \times 6.02 \times 10^{23} \times \pi(5\,\mu m/2)^2/15\,mm^2 = 80$. For the band at 612 cm^{-1}, I_{SERS}/I_{Ref} was 1. Therefore the enhancement factor for the band at 612 cm^{-1} is calculated to be 4.4×10^8. Compared to the Ag micro-hemisphere substrate (with enhancement factor of 7×10^7) [29], this Ag nanoplate-assembled film gains an even higher enhancement factor. Conceivably, the nanoplate-assembled arrays on the film provide sufficient hot spots that locate on the deeper sub-10-nm gaps between the neighboring nanoplates, ensuring that the Ag nanoplate-assembled film possesses higher enhancement factor.

For practical application the SERS substrates are required to have both high sensitivity and good reproducibility. The SERS signals achieved from six points randomly chosen on the Ag nanoplate-assembled film are very similar, as shown in Fig. 4b. Most other points investigated under the same experimental conditions can give quite similar SERS signals of R6G molecules. Therefore, the nanoplate-assembled film has indeed shown good reproducibility for the SERS measurements besides high sensitivity.

3.4. Detection of PCB-77

3.4.1. Detection of PCB-77 by the bare Ag nanoplate-assembled film

Then the nanoplate-assembled film was used as an effective SERS substrate for the detection of PCBs that belong to one kind of persistent organic pollutants as defined in the Stockholm Convention [44]. Fig. 5a shows the SERS spectra of PCB-77 at different concentrations on the Ag nanoplate-assembled film, as well as the normal Raman spectrum of PCB-77 powder for comparison. There are five distinct bands at 677 cm^{-1} (C–Cl stretching) [45,46], 1034 cm^{-1} (ring breathing) [47], 1246 cm^{-1} (C–H wagging) [46], 1298 cm^{-1} (biphenyl C–C bridge stretching) [45,46], and 1599 cm^{-1} (ring stretching) [47] in the SERS spectra (curves 2–4 in Fig. 5a), which correspond well with the normal Raman spectrum of PCB-77 (curve 1 in Fig. 5a). A linear dependence was found between the logarithmic concentrations of PCB-77 and the intensities of the fingerprint peaks (1599 cm^{-1}) (Fig. 5b) as shown below.

$$\log\ I = 5.28 + 0.505\ \log\ C \quad (3)$$

where I is the peak intensity of the SERS spectra of PCB-77 (counts), and C is the concentration of PCB-77 (M). The detection limit for PCB-77 is estimated to be 10^{-6} M.

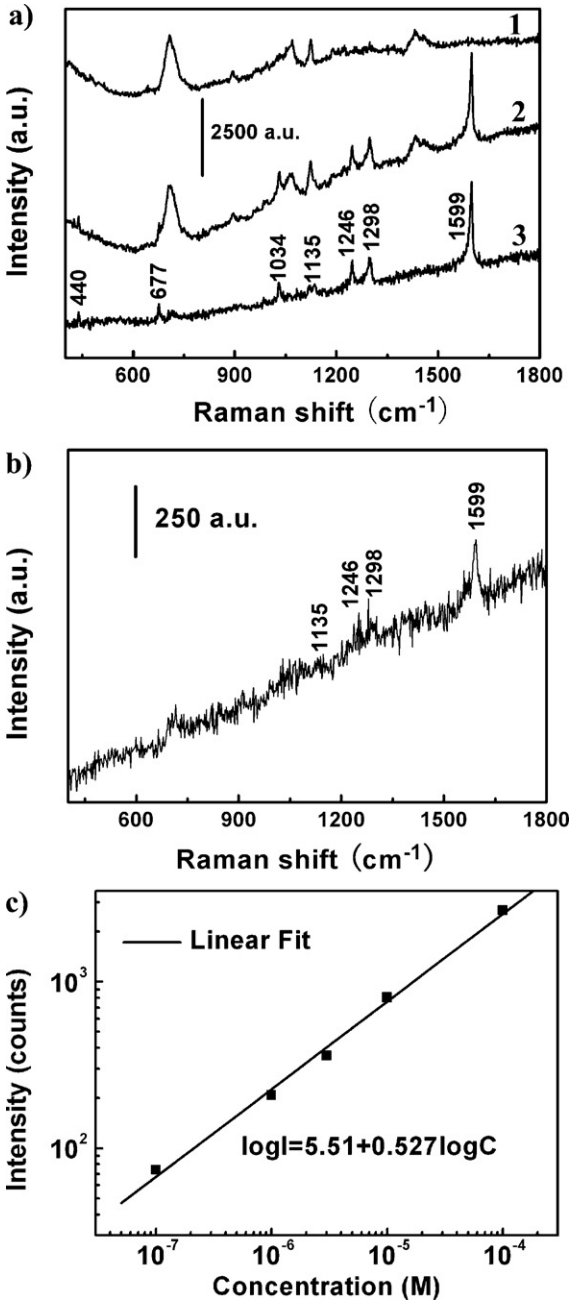

Fig. 6. (a) SERS spectra of decanethiol-modified Ag nanoplate-assembled film (curve 1) before, and (curve 2) after 10^{-4} M PCB-77 being dispersed on it, and the spectrum difference (curve 3) of (curve 1) subtracted from (curve 2). (b) SERS spectrum of 10^{-7} M PCB-77 obtained using the decanethiol-modified Ag nanoplate-assembled film as a SERS substrate. The spectra were acquired with acquisition time of 60 s. (c) The linear relationship between the logarithmic intensities (1599 cm^{-1}) and the concentrations of PCB-77 detected by using the decanethiol-modified Ag nanoplate-assembled film.

3.4.2. Detection of PCB-77 by the decanethio-modified Ag nanopalte-assembled film

As PCBs cannot be easily adsorbed onto the surface of Ag, and a partition layer (decanethiol self-assembled layer) could be assembled onto the Ag SERS substrate to capture the target PCBs molecules within the surface of the SERS substrate through its efficient van der Waals interactions with the hydrophobic PCBs [45], therefore we tried to modify our Ag nanoplate-assembled SERS substrate with decanethiol to efficiently capture the PCBs molecules and further reduce the detection limit. Fig. 6a shows the

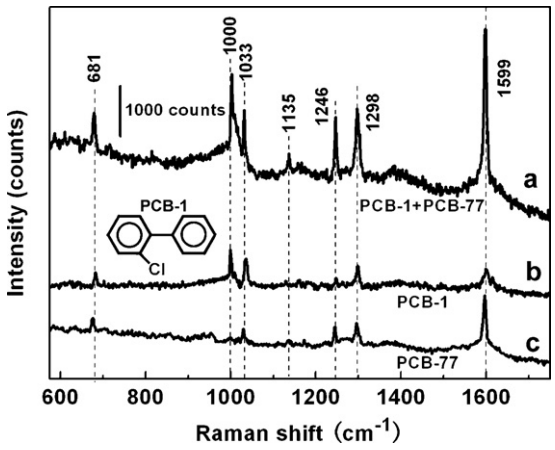

Fig. 7. Curves a–c: SERS spectra of (a) 2×10^{-4} M PCB-77 mixed with 2×10^{-4} M PCB-1, (b) 10^{-4} M PCB-1 and (c) 10^{-4} M PCB-77 detected by using the Ag nanoplate-assembled film. The spectra were acquired with acquisition time of 60 s.

SERS spectra of PCB-77 on the decanethiol-modified Ag nanoplate-assembled film. Comparing curve 3 in Fig. 6a with curve 2 in Fig. 5a, it can be concluded that the peak intensities of PCB-77 are increased about 1.5 times after decanethiol modification, indicating that the decanethiol self-assembled layer can indeed concentrate the target PCB molecules within the surfaces of the SERS substrate. When the PCB-77 concentration was decreased to 10^{-7} M, the 1137, 1246, 1296, and 1599 cm^{-1} bands (Fig. 6b) could still be identified, though their intensities decreased significantly. This detection limit of PCB-77 can be further improved if better attachment of PCB-77 to the SERS substrate can be achieved. A linear dependence was found between the logarithmic concentrations of PCB-77 and the intensities of the fingerprint peaks (Fig. 6c) as shown below.

$$\log\ I = 5.51 + 0.527\ \log\ C \quad (4)$$

where I is the peak intensity of the SERS spectra of PCB-77 (counts), and C is the concentration of PCB-77 (M). Therefore, the Ag nanoplate-assembled films indeed show the potential to be applied as sensitive and robust SERS substrates in the detection of trace PCBs after being modified with decanethiol.

3.4.3. Detection of PCB-1 and PCB-77 in their mixed solution

To show its ability to distinguish different PCBs in a mixed solution, the experiment for probing both PCB-1 and PCB-77 in their mixed solution using Ag nanoplate-assembled film has been tried. Fig. 7 shows the SERS spectra of PCB-77 mixed with PCB-1 (curve *a*), PCB-1 (curve *b*) and PCB-77 (curve *c*). Comparing curves *a*–*c*, it can be identified that the SERS spectra from PCB-1 and PCB-77 are different although many characteristic peaks of them are similar. The peak of 1000 cm^{-1} is assigned to PCB-1 while that of 1135 cm^{-1} is assigned to PCB-77. This experiment thus shows the potential of applying the SERS technique to actual measurements of some real samples if some necessary pretreatments are provided.

4. Conclusions

In summary, vertically aligned Ag nanoplate-assembled films have been achieved by spin-coating Ag seeds on an ITO substrate and subsequent electrodeposition in a mixed aqueous electrolyte of $AgNO_3$ and citric acid. The nanoplate-assembled film comprises sufficient hot spots that are uniformly distributed on the sub-10-nm gaps between the neighboring nanoplates. Such small gaps are very critical to achieve highly enhanced SERS signals. Our work has demonstrated that the Ag nanoplate-assembled films can be employed as robust, highly sensitive and reproducible SERS

substrates for the detection of PCB-77. A linear dependence was found between the logarithmic concentrations of PCB-77 and the intensities of the fingerprint peaks. The detection limit of PCB-77 can be further reduced to 10^{-7} M by decanethiol modification on the surface of the Ag nanoplate-assembled film. Therefore the vertically aligned Ag nanoplate-assembled films have potentials as SERS substrates in rapid, sensitive, and direct detection of trace PCBs.

Acknowledgements

This work was financially supported by the National Basic Research Program of China (Grant 2007CB936601), and the National Natural Science Foundation of China (Grants 50972145 and 10975152).

References

[1] S. Akzinnay, F. Bisaro, C.S. Cazin, Highly efficient catalytic hydrodehalogenation of polychlorinated biphenyls (PCBs), Chem. Commun. (2009) 5752–5753.
[2] P.G. Shields, Understanding population and individual risk assessment: the case of polychlorinated biphenyls, Cancer Epidemiol. Biomarkers Prev. 15 (2006) 830–839.
[3] R. Quiroz, P. Popp, R. Barra, Analysis of PCB levels in snow from the Aconcagua Mountain (Southern Andes) using the stir bar sorptive extraction, Environ. Chem. Lett. 7 (2009) 283–288.
[4] D.L. Lewis, A.W. Garrison, K.E. Wommack, A. Whittemore, P. Steudler, J. Melillo, Influence of environmental changes on degradation of chiral pollutants in soils, Nature 401 (1999) 898–901.
[5] G.G. Ying, C.A. Rawson, R.S. Kookana, M.S. Warne, P.A. Peng, X.M. Li, E. Laginestra, L.A. Tremblay, J.C. Chapmanf, R.P. Lim, Distribution of inorganic and organic contaminants in sediments from Sydney Olympic Park and the surrounding Sydney metropolitan area, J. Environ. Monit. 11 (2009) 1687–1696.
[6] T.M. Sandanger, E.E. Anda, A.A. Dudarev, E. Nieboer, A.V. Konoplev, S.V. Vlasov, J. Weber, J.Ø. Odland, V.P. Chashchin, Combining data sets of organochlorines (OCs) in human plasma for the Russian Arctic, Sci Total Environ. 407 (2009) 5216–5222.
[7] C. Chaemfa, J.L. Barber, K.S. Kim, T. Harner, K.C. Jones, Further studies on the uptake of persistent organic pollutants (POPs) by polyurethane foam disk passive air samplers, Atmos. Environ. 43 (2009) 3843–3849.
[8] M. Noël, L. Barrett-Lennard, C. Guinet, N. Dangerfield, P.S. Ross, Persistent organic pollutants (POPs) in killer whales (*Orcinus orca*) from the Crozet Archipelago, southern Indian Ocean, Mar. Environ. Res. 68 (2009) 196–202.
[9] G.J. Hu, C. Sun, J. Li, Y.G. Zhao, H. Wang, Y.Q. Li, POPs accumulated in fish and benthos bodies taken from Yangtze River in Jiangsu area, Ecotoxicology 18 (2009) 647–651.
[10] E.M. Krümmel, R.W. Macdonald, L.E. Kimpe, I. Gregory-Eaves, M.J. Demers, J.P. Smol, B. Finney, J.M. Blais, Delivery of pollutants by spawning salmon, Nature 425 (2003) 255–256.
[11] T.Z. Zheng, T.R. Holford, J. Tessari, S.T. Mayne, P.H. Owens, B. Ward, D. Carter, P. Boyle, R. Dubrow, S. Archibeque-Engle, S.H. Zahm, Breast cancer risk associated with congeners of polychlorinated biphenyls, Am. J. Epidemiol. 152 (2000) 50–58.
[12] L. Rylander, U. Strömberg, E. Dyremark, C. Östman, P. Nilsson-Ehle, L. Hagmar, Polychlorinated biphenyls in blood plasma among Swedish female fish consumers in relation to low birth weight, Am. J. Epidemiol. 147 (1998) 493–502.
[13] J.L. Daniels, M.P. Longnecker, M.A. Klebanoff, K.A. Gray, J.W. Brock, H.B. Zhou, Z. Chen, L.L. Needham, Prenatal exposure to low-level polychlorinated biphenyls in relation to mental and motor development at 8 months, Am. J. Epidemiol. 157 (2003) 485–492.
[14] S.K. Sagiv, S.W. Thurston, D.C. Bellinger, P.E. Tolbert, L.M. Altshul, S.A. Korrick, Prenatal organochlorine exposure and behaviors associated with attention deficit hyperactivity disorder in school-aged children, Am. J. Epidemiol. 171 (2010) 593–601.
[15] M.D. Mullin, C.M. Pochini, S. McCrindle, M. Romkes, S.H. Safe, L.M. Safe, High-resolution, PCB analysis: synthesis and chromatographic properties of all 209 PCB congeners, Environ. Sci. Technol. 18 (1984) 468–476.
[16] USEPA, Method 1668B, 2008, www.epa.gov/waterscience/methods/method/files/1668.pdf.
[17] USEPA, Method 4020, OSW, Ed., 2003, www.epa.gov/osw/hazard/testmethods/sw846/pdfs/4020.pdf.
[18] Environmental Protection Agency, www.epa.gov/pcb, 2007.
[19] K. Kneipp, H. Kneipp, I. Itzkan, R. Dasari, M. Feld, Ultrasensitive chemical analysis by Raman spectroscopy, Chem. Rev. 99 (1999) 2957–2975.
[20] H. Im, K.C. Bantz, N.C. Lindquist, C.L. Haynes, S. Oh, Vertically oriented sub-10-nm plasmonic nanogap arrays, Nano Lett. 10 (2010) 2231–2236.
[21] C.H. Sun, N.C. Linn, P. Jiang, Templated fabrication of periodic metallic nanopyramid arrays, Chem. Mater. 19 (2007) 4551–4556.
[22] Y. Lu, G.L. Liu, J. Kim, Y.X. Mejia, L.P. Lee, Nanophotonic crescent moon structures with sharp edge for ultrasensitive biomolecular detection by local electromagnetic field enhancement effect, Nano Lett. 5 (2005) 119–124.
[23] C.L. Haynes, A.D. McFarland, R.P. Van Duyne, Surface-enhanced Raman spectroscopy, Anal. Chem. 77 (2005) 246A–338A.
[24] S.J. Lee, Z.Q. Guan, H.X. Xu, M. Moskovits, Surface-enhanced Raman spectroscopy and nanogeometry: the plasmonic origin of SERS, J. Phys. Chem. C 111 (2007) 17985–17988.
[25] C. Mu, J.P. Zhang, D.S. Xu, Au nanoparticle arrays with tunable particle gaps by template-assisted electroless deposition for high performance surface-enhanced Raman scattering, Nanotechnology 21 (2010) 015604.
[26] Y. Wang, M. Becker, L. Wang, J.Q. Liu, R. Scholz, J. Peng, U. Gösele, S. Christiansen, D.H. Kim, M. Steinhart, Nanostructured gold films for SERS by block copolymer-templated galvanic displacement reactions, Nano Lett. 9 (2009) 2384–2389.
[27] P. Zhang, Y.Y. Guo, Surface-enhanced Raman scattering inside metal nanoshells, J. Am. Chem. Soc. 131 (2009) 3808–3809.
[28] P. Nielsen, S. Hassing, O. Albrektsen, S. Foghmoes, P. Morgen, Fabrication of large-area self-organizing gold nanostructures with sub-10 nm gaps on a porous Al_2O_3 template for application as a SERS-substrate, J. Phys. Chem. C 113 (2009) 14165–14171.
[29] C.H. Zhu, G.W. Meng, Q. Huang, Z. Zhang, Q.L. Xu, G.Q. Liu, Z.L. Huang, Z.Q. Chu, Ag nanosheet-assembled micro-hemispheres as effective SERS substrates, Chem. Commun. 47 (2011) 2709–2711.
[30] Q. Zhou, Y. Yang, J. Ni, Z.J. Zhang, Rapid detection of 2,3,3′,4,4′-pentachlorinated biphenyls by silver nanorods-enhanced Raman spectroscopy, Physica E 42 (2010) 1717–1720.
[31] A. Henglein, M. Giersig, Reduction of Pt(II) by H_2: effects of citrate and NaOH and reaction mechanism, J. Phys. Chem. B 104 (2000) 6767–6772.
[32] I. Pastoriza-Santos, L.M. Liz-Marzán, Synthesis of silver nanoprisms in DMF, Nano Lett. 2 (2002) 903–905.
[33] Y.G. Sun, Y.N. Xia, Shape-controlled synthesis of gold and silver nanoparticles, Science 298 (2002) 2176–2179.
[34] M. Maillard, P. Huang, L. Brus, Silver nanodisk growth by surface plasmon enhanced photoreduction of adsorbed [Ag+], Nano Lett. 3 (2003) 1611–1615.
[35] Y.J. Xiong, J.M. McLellan, Y.D. Yin, Y.N. Xia, Synthesis of palladium icosahedra with twinned structure by blocking oxidative etching with citric acid or citrate ions, Angew. Chem. Int. Ed. 46 (2007) 790–794.
[36] R.L. Penn, J.F. Banfield, Morphology development and crystal growth in nanocrystalline aggregates under hydrothermal conditions: insights from titania, Geochim. Cosmochim. Acta 63 (1999) 1549–1557.
[37] R.L. Penn, J.F. Banfield, Imperfect oriented attachment: dislocation generation in defect-free nanocrystals, Science 281 (1998) 969–971.
[38] J.X. Fang, B.J. Ding, X.P. Song, Y. Han, How a silver dendritic mesocrystal converts to a single crystal, Appl. Phys. Lett. 92 (2008) 173120.
[39] F. Huang, H.Z. Zhang, J.F. Banfield, Two-stage crystal-growth kinetics observed during hydrothermal coarsening of nanocrystalline ZnS, Nano Lett. 3 (2003) 373–378.
[40] P. Hildebrandt, M. Stockburger, Surface-enhanced resonance Raman spectroscopy of rhodamine 6G adsorbed on colloidal silver, J. Phys. Chem. 88 (1984) 5935–5944.
[41] D. Pristinski, S. Tan, M. Erol, H. Du, S. Sukhishvili, In situ SERS study of Rhodamine 6G adsorbed on individually immobilized Ag nanoparticles, J. Raman Spectrosc. 37 (2006) 762–770.
[42] H. Ko, V.V. Tsukruk, Nanoparticle-decorated nanocanals for surface-enhanced Raman scattering, Small 11 (2008) 1980–1984.
[43] M. Zamuner, D. Talaga, F. Deiss, V. Guieu, A. Kuhn, P. Ugo, N. Sojic, Fabrication of a macroporous microwell array for surface-enhanced Raman scattering, Adv. Funct. Mater. 19 (2009) 3129–3135.
[44] UNEP 2007 Annual Report, 2008, pp. 90–103.
[45] K.C. Bantz, C.L. Haynes, Surface-enhanced Raman scattering detection and discrimination of polychlorinated biphenyls, Vib. Spectrosc. 50 (2009) 29–35.
[46] G. Socrates, Infrared and Raman Characteristic Group Frequencies: Tables and Charts, 3rd ed., Wiley, New York, 2001, pp. 158–167.
[47] A. Gutés, C. Carraro, R. Maboudian, Silver dendrites from galvanic displacement on commercial aluminum foil as an effective SERS substrate, J. Am. Chem. Soc. 132 (2010) 1476–1477.